Atomic and electronic structures of neutral and cation Sn_n ($n=2-20$) clusters: A comparative theoretical study with different exchange-correlation functionals

Chiranjib Majumder,[1,*] Vijay Kumar,[2] Hiroshi Mizuseki,[3] and Yoshiyuki Kawazoe[3]
[1]*NM&SC Division, Bhabha Atomic Research Center, Trombay, Mumbai 400 085, India*
[2]*Institute for Materials Research, Tohoku University, 2-2-1 Katahira Aoba-Ku, Sendai 980-8577, Japan and Dr. Vijay Kumar Foundation, 45 Bazar Street, Chennai 600 078, India*
[3]*Institute for Materials Research, Tohoku University, 2-2-1 Katahira, Aoba-Ku, Sendai 980 8577, Japan*
(Received 17 April 2003; revised manuscript received 1 July 2004; published 3 January 2005)

The atomic structures and energetics of neutral and singly positively charged Sn_n^+ ($n=2-20$) clusters have been calculated using a plane wave pseudopotential method under the framework of the generalized gradient approximation of the density functional theory as well as by using the hybrid exchange-correlation functionals viz., BLYP, B3LYP and B3PW91 under the LCAO-MO approach. From the results a systematic analysis has been carried out to obtain the physico-chemical properties such as atomization energies, ionization potentials and fragmentation behavior of the neutral and cation clusters. A comparison with the available experimental data shows that the results obtained from the B3PW91 functional provide an overall good agreement for all the properties calculated here. Our calculations show that the dominant channel for the fragmentation of Sn_n^+, $n \leqslant 11$, clusters is the evaporation of an atom such that the charge remains on the rest of the cluster, while for larger clusters, fission into two subclusters becomes more favorable. Raman and infrared vibrational spectra have been calculated for a few selected clusters. These confirm the structural stabilities of the clusters and can provide a way to identify the atomic structures from experiments.

DOI: 10.1103/PhysRevB.71.035401 PACS number(s): 73.22.−f, 36.40.Cg, 36.40.Qv, 36.40.Ei

I. INTRODUCTION

The realization of novel cluster assembled materials requires understanding of the fundamental properties of atomic clusters.[1–4] During the past decade a large number of experimental and theoretical studies have been carried out in this direction. The structural and physico-chemical properties of the group 14 elemental clusters have been the subject of intense research because of the fundamental interest and the possibility of applications in nano-technologies. Their growth behavior and the nature of bonding differs considerably as one goes down from C to Pb. Much attention has been focused on understanding the structural similarities and differences among Si, Ge, Sn and Pb clusters. The atomic structures of the group 14 elemental clusters adopt geometries ranging from chain, fullerene cages and nanotubes for carbon[5] and noncompact prolate structures for Si and Ge[6–8] to compact structures for Pb. Structures of Si and Ge clusters progressively undergo rearrangements with an increase in size and transform into a 3D growth. However, this has not yet been well understood. Recently tin clusters have become the center of focus due to the report of their abnormal higher melting temperatures[9] as compared to the bulk value. It is believed that the higher melting temperatures of tin clusters could be due to the different isomeric structures of small clusters as compared to the bulk. In a bulk material, the melting process initiates at the surface and small clusters have most of their atoms on the surface. Therefore, knowledge of the atomic structures and bonding nature are necessary for a proper understanding of the melting behavior in such small clusters. Tin is unique as it exists both in covalent (α) and metallic (β) bulk phases. Therefore, the evolution of the bonding nature in clusters could show such a different behavior. In the periodic table, tin is below germanium and above lead. It is, therefore, not surprising that the mass spectrum of tin clusters shows similarities with those of germanium and lead clusters.[10] Although some experimental reports are also available on ionization potentials (IPs) of tin clusters, very little is known about the structures and stabilities of the charged clusters.

Gas phase tin clusters were first detected in vapor in equilibrium with molten tin by Gingerich and co-workers.[11] Enhanced stability of clusters containing multiples of three tin atoms, i.e., Sn_3 and Sn_6 was predicted. Martin and Schabar[12] have reported mass distribution of tin clusters using the time of flight mass spectrometry. The mass spectrum produced by the ionization of the condensed elemental vapor was found to resemble that of Pb_n, but not that of Ge_n. This indicated metallic behavior of tin clusters rather than semiconducting. In contrast to this, Noda and co-workers[13,14] have reported mass spectrum of tin clusters that resembles those of Si_n and Ge_n clusters but different from that of Pb_n. In these experiments the mass spectra for Si_n, Ge_n, Sn_n, and Pb_n clusters were generated using the same conditions. This fact was further supported by the photoelectron spectroscopy studies of Sn_n^- clusters which revealed similar electronic structures of Si_n^-, Ge_n^- and Sn_n^- clusters that differed from those of Pb_n^- clusters.[15,16] These experiments led to the conclusion that tin clusters are covalently bonded and are not metallic-like. However, it should be mentioned that the mass abundance spectra are strongly dependent on the source conditions. The contrasting behavior of tin mass spectrum in the above studies could be argued to be due to a change in the source conditions. Duncan and co-workers[10] have surveyed the abundance of Sn_n clusters produced by laser vaporization of β-tin under various conditions and concluded that Sn clusters

have properties intermediate to those of Ge and Pb clusters.

Yoshida and Fuke[17] have measured the IPs of Si_n, Ge_n and Sn_n clusters using laser photoionization and time-of-flight mass spectrometry for ionization and detection of clusters, respectively. Their results show very similar size dependence of IPs for germanium and tin clusters having fewer than 12 atoms. However, a sharp decrease observed in the IPs for Ge_n clusters between $n=15$ and 26, consistent with silicon clusters, was not found for tin clusters. The IPs of tin clusters in the medium size range ($n=15-41$) show a gradual decrease without any sharp change. These differences in the IPs have been explained to be due to possibily a different structural growth of Sn_n clusters as compared to those of Si_n and Ge_n. The chemical reactivity of small Sn_n ($n\leqslant 9$) anions towards oxygen, nitrous oxide, hydrogen sulfide, ethane, and several simple alcohols has been determined.[18,19] However, this could not lead to any structural inferences. Jarrold and co-workers[6–9,20,21] have characterized the structures of Si_n, Ge_n, Sn_n and Pb_n clusters using ion mobility measurements. It is observed that the growth patterns of silicon, germenium and tin clusters adopt prolate structures in small cluster region. However, for lead clusters, near-spherical structures have been observed for all cluster sizes. In the small size range Sn_n clusters start deviating from those of Si_n above $n=14$ and of Ge_n above $n=21$. In the range of 35–65 atoms, tin clusters gradually rearrange themselves towards near spherical geometries, passing through several intermediate structural transitions. So the transition to "normal" metal cluster growth in group 14 elements occurs between tin and lead, one row lower than the transition from covalent to metallic bonding in bulk solids under ambient conditions.

Theoretical studies of the electronic and atomic structures of small Sn_n neutral and anion clusters have been carried out using molecular orbital (MO) method and density functional theory.[19,22–27] These results predict the lowest energy structures for Sn_n neutral clusters with $n\leqslant 7$ to be identical to those reported previously for Si_n (Refs. 28–30) and Ge_n (Refs. 31 and 32) clusters. Also the structural and dynamical properties of C_n, Si_n, Ge_n and Sn_n clusters have been investigated by Lu *et al.*[33] using the local density approximation (LDA). They found that for $n\leqslant 7$, and $n=10$ and 12, Si_n, Ge_n and Sn_n clusters share similar structures. However, for Sn_8 and Sn_9 different structures have been obtained as compared to those of the corresponding silicon and germanium clusters. A detailed study of the low lying isomers of neutral Sn clusters having upto 20 atoms has been carried out by us[34] and deviations from the growth behavior in the range of $n>14$ have been identified. Here we present results of the electronic and atomic structures of singly positively charged tin clusters in order to obtain the IPs as well as a better comparison with experiments that are generally performed on charged clusters.

Earlier theoretical studies on silicon clusters have shown[35] that the choice of the exchange-correlation functional plays an important role in determining the ground state properties of small clusters. It has been found that for Si_{20}, the BLYP exchange-correlation functional gives results that are in close agreement with those obtained from quantum Monte Carlo calculations. In our earlier study of neutral tin clusters, we have found[34] that the generalized gradient approximation (GGA) gives far superior binding energies (BEs) defined as $[nE(1)-E(n)]/n$, $E(n)$ being the total energy of an n atom cluster, as compared to those obtained by using LDA.[33] However, even GGA results were found to predict significantly higher BEs as compared to the experimental atomization energies available for clusters having up to 7 atoms. Motivated from these results we have carried out a detailed study of the electronic structure of neutral and cation tin clusters using different exchange-correlation functionals. A comparison of these results with the available experimental data on the stabilities, IPs and the fragmentation behavior shows that the B3PW91 form of exchange-correlation functional gives a good description of the bonding in small clusters.

II. COMPUTATIONAL DETAILS

The lowest energy structures of the neutral and charged clusters have been obtained within the density functional theory using the ultrasoft pseudopotential[36,37] for the electron–ion interaction and a plane wave basis set for the wavefunctions. The GGA[38] has been used to describe the exchange-correlation energy. The ionic pseudopotential used here was also derived within the GGA so that the errors due to the core-valence exchange-correlation could be avoided.[39] The cut-off energy for the plane waves was taken to be 19.1156 Ry. Test calculations on bulk tin in the diamond structure gave the lattice constant and cohesive energy[40] to be 6.63 Å and 3.16 eV/atom that are in good agreement with the experimental values[41] of 6.49 Å and 3.14 eV/atom, respectively. A comparative study of the equilibrium properties of bulk tin has also been performed[42] within GGA and the LDA using a linear combination of atomic orbital (LCAO) method. In this work the cohesive energy is slightly underestimated while the lattice constant is slightly overestimated. We have found a similar difference for clusters as discussed below. Such small changes can arise due to the use of different basis sets as well as pseudopotentials but we believe that the overall trends will be similar. For neutral clusters, we used a simple cubic supercell of side 20 Å and the Γ point for the Brillouin zone integrations. Some of the larger clusters that are prolate in shape have been placed along the diagonal axis of the cube so that the distances between the nearest images are sufficiently large and the interactions between them are minimal. For the determination of the lowest energy isomers, the simulated annealing method is generally best suited and has been successfully used for metal clusters. However, for covalently bonded systems, it is known to fail.[44] Therefore, we optimize a large number of structures, including those reported for Si and Ge[35,43,44] clusters. For charged clusters we use a neutralizing background and a larger supercell that is required to account for the dipolar corrections. In order to take care of these corrections we have increased the cell length from 20 to 30 Å and checked that the energy convergence is achieved within 10 meV. Therefore, we have used a cubic cell of 30 Å side length for all geometry optimizations of the cation clusters. Again the larger clusters with elongated shapes are placed along the diagonal of the cube. These calculations on cation clusters

have been carried out using the *spin-polarized* GGA due to the odd number of electrons. The spin multiplicity of all cation clusters is 2.

The geometry optimizations have also been carried out for a few selected clusters using the LCAO-MO real space method with similar type of exchange-correlation functional (PW91PW91) and the Los Alamos National Laboratory effective core potentials with double-zeta valence (Lanl2DZ) basis set as implemented in the Gaussian-98 program.[45] A comparison between these two results suggests that the average interatomic distances between nearest neighbors increase ($\approx 2-3\%$) in the LCAO-MO method and there is a decrease in the average BE. In order to understand the effects of different exchange-correlation functionals on the electronic and atomic structures of these clusters, further calculations have been carried out on the neutral and cation clusters employing three different hybrid exchange-correlation functionals[46] viz., BLYP, B3LYP and B3PW91 using the LCAO-MO approach available in the Gaussian-98 program.[45] The Lanl2DZ basis functions and effective core potential were again used for tin.[47,48] Presently, it is one of the most powerful methods to deal with heavier elements like Sn clusters. For the purpose of comparing results obtained from different exchange-correlation functional we have used the lowest energy structures obtained from the GGA calculations[34] as the initial guesses. Finally, the structural stability of the lowest energy isomers of selected clusters ($n=6,7,10,16$, and 20) has been checked by performing frequency calculations. However, with the Lanl2DZ basis set, we found two and one frequencies to be negative in the case of $n=6$ and 20, respectively. Therefore, further checks were made by using a different basis set, namely the Stuttgart/Dresden effective core pseudopotential basis set which showed no negative frequency in all cases tested, signifying the stablility of the atomic structures. The atomic structures and the BEs[49] obtained by using the SDD basis set are very close to the results obtained with the Lanl2DZ basis set. For Sn_{20} the BE is only 0.1 eV more than the value obtained by using the Lanl2DZ basis set. Therefore, we believe that the general conclusions drawn on the basis of the Lanl2DZ basis set will hold.

III. RESULTS

A. Ground state geometries of neutral and cation tin clusters

In this section we first describe the lowest energy atomic structures of the neutral and cation tin clusters obtained from the plane wave pseudopotential calculations. This is followed by a brief discussion of the atomic structures obtained by using the B3PW91 hybrid exchange-correlation functional with the LCAO-MO method. The reason for choosing the B3PW91 energy functional is its better agreement with the available experimental results on small clusters.

The structures of neutral tin clusters ($n=2-20$) obtained from the plane wave pseudopotential approach have been reported earlier.[34] Here we present atomic structures of cation tin clusters obtained with the same method in order to understand the charging effects on the structure of neutral clusters. In Fig. 1 we have presented the lowest energy structures of tin cation clusters with n up to 10. The effects of a single positive charge on the geometries of larger clusters are less and hence we do not discuss them in detail except for their electronic structures that is described in the following section. Although the structures of the cation clusters are similar to those of their neutral counterparts in general, there are distortions due to the polarization of the electron spin charge density. The interatomic distances between the nearest neighbors do not reflect any systematic increasing or decreasing trend when structures of neutral and cation clusters are compared. For example, in the case of $n=2,3,8$, and 9, the mean interatomic distances increase from 2.78, 2.68, 2.82, and 2.95 Å for the neutral clusters to 2.82, 2.80, 3.01, and 3.00 Å, respectively, for the cation clusters. The opposite trend is, however, observed for $n=4$, 5, 6, and 7, i.e., the mean nearest neighbor distances decrease from 2.83, 2.83, 2.91, and 3.03 Å for the neutral clusters to 2.82, 2.78, 2.87 and 2.93 Å, respectively, for the cation clusters within GGA. Similar features in the lowest energy structures of Sn_4^+ and Sn_5^+ were also obtained by Balasubramanian and co-workers[23] from *ab initio* quantum chemical studies using CASSCF (*complete active space multiconfiguration self-consistent-field method*) and MRSDCI (*multireference singles + doubles configuration interaction*) level of theory. According to their results for Sn_4 and Sn_4^+ clusters, rhombus structures with an acute apex angle of 63.4° and 71.8°, respectively, have the lowest energies. Our results obtained by the plane wave pseudopotential method (acute apex angle for Sn_4 and Sn_4^+ being 63.2°and 71.8°, respectively) are in very good agreement with these calculations.

As the structural relaxation in cation clusters is generally small, further single point energy calculations were performed using the hybrid exchange-correlation energy functionals (BLYP, B3LYP, B3PW91) in the Gaussian program by taking the optimized geometries obtained from the plane

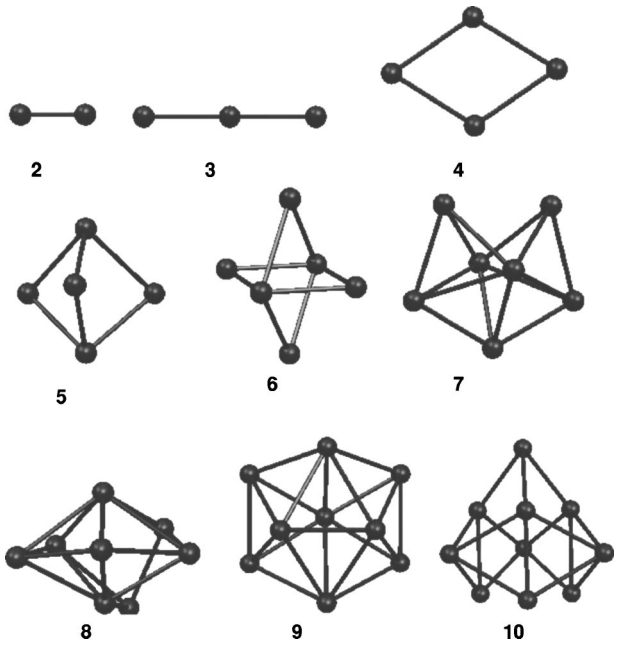

FIG. 1. Lowest energy structures of Sn_n, $n=1-10$, cation clusters.

TABLE I. Mean nearest neighbor bond lengths (Å) for small neutral and cation tin clusters obtained from different exchange-correlation functionals.

n	GGA neutral	GGA cation	B3PW91 neutral	B3PW91 cation
2	2.78	2.82	2.70	3.07
3	2.68	2.80	2.73	2.67
4	2.83	2.82	2.86	3.15
5	2.83	2.78	2.90	2.84
6	2.91	2.86	2.99	2.92
7	3.04	2.93	3.10	2.98
8	2.82	3.01	2.86	3.05
9	2.95	3.00	3.03	3.06
10	2.90	2.93	2.95	2.99

wave pseudopotential method in order to obtain the effects of different hybrid functionals on energy. Such calculations reveal that B3PW91 functional gives closer agreement with experiments for small clusters for which experimental data of the BEs are also available. Therefore, structural optimizations were further carried out for neutral and cation tin clusters using B3PW91 energy functional. As expected the relaxation energy is again found to be small (the largest value of the relaxation energy is found to be 0.18 eV) among all the cases. In general, the structures of the neutral and cation clusters are not significantly different except for the very small clusters where the effects of the positive charge are expected to be large. For comparison, we have listed the mean nearest neighbor bond lengths in Sn_n (n up to 10) clusters in Table I. It is noted that for clusters with $n=2$ and 3, the effects of the different exchange-correlation functionals are quite significant. For Sn_2^+ the increase in the bond length within B3PW91 is much larger than in GGA. Also for Sn_4^+, there is a significant increase in the mean bond length using B3PW91 while in GGA there is a very small decrease. The reverse is found for $n=3$. In GGA there is an increase in the mean bond length for the cation cluster while in B3PW91, there is a significant decrease.

An interesting case is the cation of Sn_3 which has a linear chain structure as compared to a triangular one for the neutral. An isosceles triangle with 67° angle is 0.14 eV higher in energy as compared to the linear chain. In other cases the structural differences are small. First, for neutral Sn_5, GGA gives elongated trigonal bipyramid to be of lowest energy. Its base is an equilateral triangle with the bond length of 3.73 Å and the distance between the apex and base atoms is 2.83 Å while the apex to apex distance is 3.63 Å. This is similar to the result for Si_5. The B3PW91 result differs slightly with the apex to base atoms and apex to apex bond lengths of 2.91 and 3.66 Å, respectively. For Sn_5^+ there is distortion in the structure and it can be considered as a capped rhombus (Fig. 1) with the side of the rhombus to be 2.92 (3.0) Å and the bond lengths between the capping atom and the two diagonal atoms of the rhombus to be 2.79 (2.84) Å using the plane wave GGA (B3PW91 LCAO-MO) method. For Sn_6^+, the crossed rhombii structure with bond lengths of 2.99 Å for the neutral[34] distorts such that one rhombus becomes wider than the other with 3.10 and 2.92 Å bond lengths, respectively. In the case of Sn_7^+ the pentagonal bipyramid structure of the neutral cluster becomes distorted with the bond lengths between the base atoms varying from 2.98 to 3.31 Å as compared to 3.10 Å for the neutral using the B3PW91 functional. With an increase in cluster size the effects of a single positive charge on the structure become smaller (Table I).

A comparison of the structures obtained from the plane wave pseudopotential approach and B3PW91 (LCAO-MO method) results shows that the overall structures of neutral clusters remain unaltered. There are $\approx 3-4$ positively charged clusters with respect to their neutral counterparts. In order to further check the stability of the lowest energy structures of these clusters we have carried out the vibrational analysis for a few selected clusters with $n=6$, 7, 10, 16, and 20. The results of the vibrational frequencies are listed in Table II along with their respective infrared intensities and Raman activities. In all the cases all frequencies are positive, suggesting the stability of the structures. For Sn_{20}, there are very low frequency modes which are due to the prolate shape of this cluster which has two linked Sn_{10} clusters. However, in all the cases, the highest frequencies are similar. The analysis of the ground state structures for Sn_n ($n=2-20$) clusters reveals that the growth behavior of Sn clusters flip-flops between partial metal-like and silicon-type structures. The bond lengths also confirm this behavior. Some clusters have a few nearest neighbor bonds that are even longer than in bulk allotropes at the expense of some strong short bonds. In some other clusters, however, the nearest neighbor bond lengths are nearly uniform and are shorter than in the bulk as one expects for metal clusters. This picture remains also for the cation clusters.

B. Binding energies and stabilities

The BEs of neutral and cation clusters were calculated using various exchange-correlation functionals (BLYP, B3LYP, and B3PW91) under the LCAO-MO approach, keeping the plane wave based optimized atomic structures fixed. Table III summarizes these results.[40] It is clear that the results obtained from B3PW91 exchange-correlation functional are in good agreement with the available experimental BEs[11] in the small size range. Full geometry optimizations of all the clusters using the B3PW91 exchange-correlation functional and a few "magic" clusters that are relatively more stable than the adjacent clusters, using BLYP, B3LYP hybrid exchange-correlation functionals, also showed only small changes in the binding energies upon relaxation. The results are listed in Table IV for the "magic" clusters. Figure 2 shows the BE plots as a function of the inverse cube root of the number of atoms in a cluster using different exchange-correlation functionals. It is seen that BLYP, B3LYP, and B3PW91 functionals underestimate the BEs as compared to the experimental values, while pseudopotential calculations using GGA overestimate the BEs. An extrapolation[50] of these results to the bulk cohesive energy shows that GGA would give a better description of bonding in large clusters. This is

TABLE II. Point group symmetries, vibrational frequencies (cm^{-1}) and IR intensities as well as Raman activity for the ground state structures of Sn_n (n=4,6,7,10,16,20) neutral clusters.

System	Symmetry	Vibrational frequency (IR intensity, Raman activity)
4	D_{2h}	32.90 (0.28, 0.0), 79.77 (0.03, 0.0), 118.92 (0.0, 22.35), 160.229 (0.0, 6.28), 173.473 (0.0, 70.43), 185.197 (11.67, 0.0)
6	C_{2v}	20.420 (0.04, 0.0), 20.435 (0.04, 0.0), 53.178 (0.0, 0.0), 91.126 (0.08.63), 106.966 (0.0, 19.9), 121.741 (0.39, 0.0), 137.681 (0.0, 16.53), 147.730 (0.0, 3.07),147.743 (0.0, 3.07), 169.217 (2.99, 0.0), 169.2189 (2.99, 0.0), 175.169 (0.0, 69.23)
7	D_{5h}	57.901 (0.0, 0.0), 58.106 (0.0, 0.0), 82.684 (0.016, 0.0), 82.736 (0.016, 0.0), 85.375 (0.19, 0.0), 108.402 (0.0, 6.6), 108.466 (0.0, 6.53), 126.473 (0.0, 3.30), 126.519 (0.0, 3.30), 127.947 (0.0, 28.20), 31.878 (0.0, 3.18), 131.937 (0.0, 3.18), 162.247 (2.38, 0.0), 162.307 (2.34, 0.0), 167.5414 (0.0, 61.17)
10	C_{3v}	28.763 (0.01, 0.13), 29.244 (0.149, 0.132), 71.515 (0.008, 0.161), 71.5940 (0.006, 0.016), 76.9270 (0.001, 1.94), 79.6248 (0.08, 4.24), 79.7755 (0.08, 4.30), 94.5170 (0.002, 0.015), 97.6989 (0.07, 8.14), 97.8883 (0.06, 8.11), 99.9682 (0.19, 5.38), 101.7495 (0.22, 2.10), 101.976 (0.215, 2.20), 110.386 (0.05, 11.94), 119.667 (0.015,0.28), 119.944 (0.015, 0.3), 124.114 (0.0, 0.01), 133.845 (0.07, 7.80), 140.789 (0.08, 74.58), 146.389 (0.00, 0.40), 146.746 (0.00, 0.42), 161.054 (0.97, 2.40), 161.322 (0.97,2.37), 182.303 (0.73, 6.79)
16	C_{2v}	20.987 (0.0, 0.63), 26.146 (0.08, 0.02), 30.874 (0.0, 0.09), 35.923 (0.015, 2.01), 38.331 (0.34,58), 57.030 (0.25, 3.60), 61.448 (0.01,12.70), 61.745 (0.0, 8.33), 66.559 (0.02, 0.037), 73.659 (0.017, 8.39), 73.719 (0.01, 3.57), 75.066 (0.08,0.37) 75.476 (0.0, 2.21), 80.828 (0.05, 0.91), 80.978 (0.028, 0.64), 86.484 (0.037, 0.11), 89.016 (0.52, 0.04), 91.314 (0.03, 0.88), 92.618 (0.23, 7.99), 92.694 (0.0, 7.76), 5.688 (0.01, 5.15), 98.526 (0.02, 1.45), 99.688 (0.12, 3.94), 103.143 (0.3, 7.42), 105.415 (0.12, 3.33), 108.150 (0.0, 0.0), 110.169 (0.07, 1.90), 111.097 (0.30, 0.63), 112.430 (0.06, 20.9), 122.218 (0.6, 0.7), 128.084 (1.5, 0.44), 130.612 (0.0, 1.16), 132.246 (0.2, 81.3), 133.962 (1.38, 2.2), 140.218 (0.3, 1.3), 141.115 (2.3, 1.66), 150.039 (0.13, 0.35), 156.918 (0.8, 2.13), 167.252 (1.4, 0.46), 168.198 (0.22, 4.1), 168.836 (0.0,6.06), 174.882 (0.13, 2.97)
20	C_s	3.237 (0.0,0.05), 8.824 (0.01,0.28), 9.546 (0.0, 1.0), 12.725 (0.43, 1.17), 22.426 (0.0, 7.2), 26.429 (0.0, 2.8), 36.128 (0.05, 1.25), 36.409 (0.0, 1.28), 38.749 (0.03, 0.91), 40.053 (0.21, 0.11), 64.334 (0.0, 0.9), 66.296 (0.4, 0.14), 68.913 (0.0, 21.30), 9.449 (0.65, 0.1), 75.811 (0.0 4.62), 76.100 (0.01, 0.8), 77.244 (0.11, 6.12), 78.794 (0.01, 4.80), 80.549 (1.04, 0.52), 80.867 (0.02, 25.89), 92.037 (0.06, 31.46), 93.869 (3.4, 0.04), 94.746 (1.26, 0.07), 95.080 (0.05, 0.69), 95.641 (3.50, 1.30), 96.982 (0.22, 15.35), 97.412 (0.65, 8.92), 98.885 (0.06, 118.14), 99.00 (0.20, 20.0), 99.996 (0.2, 2.60), 101.710 (0.22, 18.09), 103.409 (0.388, 0.79), 105.797 (8.92, 0.15), 106.718 (0.0, 15.82), 117.835 (0.01, 1.01), 118.983 (0.2, 0.03), 120.024 (0.09, 0.2), 121.791 (0.0, 0.15), 125.446 (0.0, 0.9), 125.688 (0.0, 0.27), 126.455 (0.0, 23.36), 128.072 (2.24, 0.12), 136.221 (0.0, 0.65), 137.214 (0.0, 291.81), 138.466 (0.0, 30.47), 140.545 (0.32, 0.30), 141.236 (0.05, 0.34), 142.266 (0.01, 0.55), 158.740 (1.9, 1.7), 158.974 (0.81, 5.98), 159.140 (0.74, 5.92), 159.786 (1.74, 6.63), 177.573 (5.63, 0.02), 178.244 (0.0, 39.68)

intuitively correct as with increasing size the bonding nature in these clusters is likely to be more metallic and electron-correlation effects would become weaker. We have made an interpolation between the different calculated results as well as the experimental data on BEs of clusters and the bulk cohesive energy. We hope that this would be a good representation of the BEs of these clusters leaving aside small fluctuations due to the "magic" behavior of some clusters.

As emphasized in our earlier paper[34] an important aspect of this graph is the slow variation of the BE with size after about ten atom clusters. The small slope of the BE curve in the large cluster range reflects the low surface energy of tin and the strengthening of the bonds in clusters, particularly at the surface. The binding energy of a 20-atom cluster in plane

TABLE III. Comparison of the binding energies (eV) of Sn_n clusters using different exchange-correlation functionals under density functional theory formalism. The notation PW/PW91 represents the results form plane wave based pseudo-potential calculations, while the others are from LCAO-MO based methods. SP (OPT) represents results of single point (optimized) calculations. The gap (eV) is calculated using B3PW91 functional with optimized geometries. Experimental values (eV) are taken from Ref. 8.

System	PW/PW91-OPT	BLYP-SP	B3LYP-SP	B3PW91-SP	B3PW91-OPT	Exp.	Gap
Sn_2	1.29	1.10	0.88	0.91	0.93	0.94	1.44
Sn_3	1.85	1.53	1.34	1.46	1.47	1.65	1.95
Sn_4	2.30	1.86	1.75	1.85	1.90	1.94	1.08
Sn_5	2.48	1.97	1.86	2.0	2.02	2.11	2.52
Sn_6	2.65	2.07	1.97	2.15	2.17	2.28	2.49
Sn_7	2.77	2.15	2.07	2.27	2.29	2.37	2.42
Sn_8	2.71	2.10	2.01	2.21	2.23		1.88
Sn_9	2.79	2.15	2.06	2.28	2.30		2.27
Sn_{10}	2.85	2.21	2.14	2.36	2.38		2.29
Sn_{11}	2.79	2.15	2.06	2.29	2.31		1.70
Sn_{12}	2.79	2.15	2.07	2.30	2.32		1.79
Sn_{13}	2.80	2.15	2.07	2.30	2.33		1.68
Sn_{14}	2.85	2.22	2.15	2.39	2.41		2.11
Sn_{15}	2.86	2.20	2.14	2.38	2.40		1.35
Sn_{16}	2.87	2.23	2.16	2.41	2.44		2.08
Sn_{17}	2.84	2.18	2.10	2.35	2.37		1.68
Sn_{18}	2.86	2.21	2.14	2.39	2.40		1.49
Sn_{19}	2.85	2.19	2.14	2.38	2.39		1.26
Sn_{20}	2.87	2.23	2.16	2.40	2.41		1.55

wave GGA calculation is only about 10% less as compared to the bulk value. On the other hand, if we take the B3PW91 result, then the BE of the 20-atom cluster is about 25% less than the bulk plane wave GGA calculation which is very close to the experimental value. Since in this size range the B3PW91 result is a significantly under estimation, we believe the more realistic value would be in between as we have shown from the interpolated result. This would then suggest that the BE of clusters in this size range would be about 15–20% less than the bulk value. This is significantly less as compared to over 20%, e.g., for aluminum clusters.[51] We feel it to be important in the understanding of the melting behavior of these clusters. It is also noticed that the energy gap between the highest occupied–lowest unoccupied molecular orbitals (HOMO–LUMO) is higher in the case of the B3PW91 functional as compared to the value obtained from the GGA calculations[34] (Table III). As it is well known, the GGA functional is generally expected to underestimate the HOMO–LUMO gaps and we hope that B3PW91 results provide a more realistic estimate.

We have also calculated the second order difference in energy, defined as $\Delta_2(n)=E(n+1)+E(n-1)-2E(n)$, of the neutral and cation clusters obtained from the B3PW91 functional. These are shown in Fig. 3. It is found that cation clusters with 8, 11, 12 and 17 atoms tend to gain significant stability with respect to their corresponding neutrals. In contrast, clusters with 7, 10 and 16 atoms that are "magic" in the neutral state tend to become less stable in the cation state. This could be a possible reason that at high laser fluence 8 and 11 atom cation clusters show high abundances.[52] Further,

TABLE IV. Binding energies (BE) in eV and bond lengths (BL) in Å for optimized structures of a few magic clusters obtained by using different exchange-correlation functionals.

	BLYP		B3LYP		B3PW91		PW/PW91		Exp.	
	BE	BL	BE	BL	BE	BL	BE	BL	BE	BL
Sn_2	1.13	2.90	0.89	2.71	0.93	2.70	1.29	2.78	0.94	2.74
Sn_4	1.92	2.91	1.80	2.88	1.90	2.90	2.30	2.85	1.94	
Sn_7	2.20	3.16	2.10	3.13	2.29	3.10	2.77	3.03	2.43	
Sn_{10}	2.26		2.17		2.38		2.85	2.90		

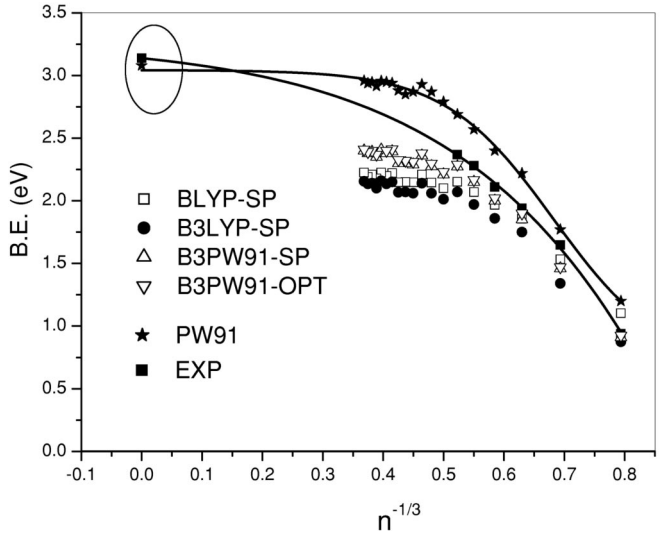

FIG. 2. Binding energies of tin clusters as a function of $n^{-1/3}$ using different exchange-correlation functionals. Note that GGA curve (upper) overestimates the binding energies while the hybrid functionals underestimate these as compared to the experimental values. An interpolation curve (lower) has been drawn between these results and the bulk cohesive energy.

the abundances would also depend on the fragmentation behavior of the cation clusters that is discussed in the following sections.

In order to understand the electronic structure of clusters we have shown results of the density of states for 7-, 10-, 16-, and 20-atom neutral and 8-, 10-, 11-, and 20-atom cation clusters obtained from the Gaussian method (Figs. 4 and 5). All neutral clusters have significant HOMO–LUMO gaps and for 7- and 10-atom clusters the spectra are sharper due to their symmetric shapes. Comparing the electronic spectra of 10 and 20, we find that the main features in the two spectra are similar, but for the 20-atom cluster, the degeneracies are lifted and the states are more spread. This also results in a smaller HOMO–LUMO gap for Sn_{20}. For cation clusters, we

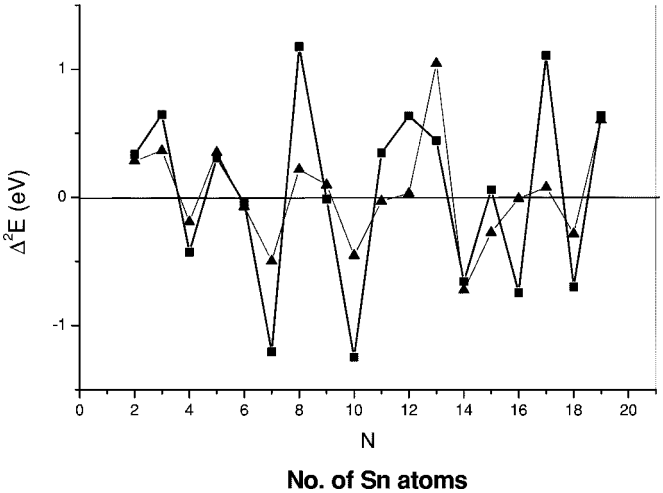

FIG. 3. Second order difference in energy for neutral (square) and cation (triangle) tin clusters. A positive value indicates "magic" cluster.

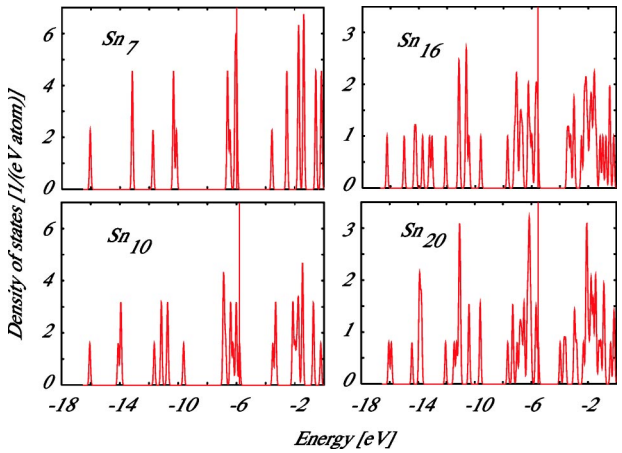

FIG. 4. Plots of the density of states for Sn_7, Sn_{10}, Sn_{16} and Sn_{20} neutral clusters in the lowest energy structures. The HOMO energy is indicated by vertical dotted line.

find significant HOMO–LUMO gaps for 8- and 11-atom clusters and this also favors the "magic" nature of these clusters as compared to the neutral ones. On the other hand, the HOMO–LUMO gaps for 10- and 20-atom clusters are smaller as compared to the values for 8- and 11-atom clusters. This is in line also with the reduced "magic" nature of these clusters. As a whole the spectra are shifted to higher binding energies due to the presence of a positive charge. However, this shift is smaller for Sn_{20} as the positive charge is distributed over two 10-atom clusters.

C. Ionization potentials

Adiabatic IPs for tin clusters up to 20 atoms have been reported recently[53] using the GGA[38] and plane wave pseudopotential approach. These results underestimated the IP values as compared to those obtained from experiments. Here we present the adiabatic IPs calculated using the B3PW91 functional. First of all, the IP of a tin atom is calculated to be 6.91 and 7.52 eV, respectively, with GGA and B3PW91 functionals. The B3PW91 result is closer to the experimental value of 7.29 eV. This gives further support that the

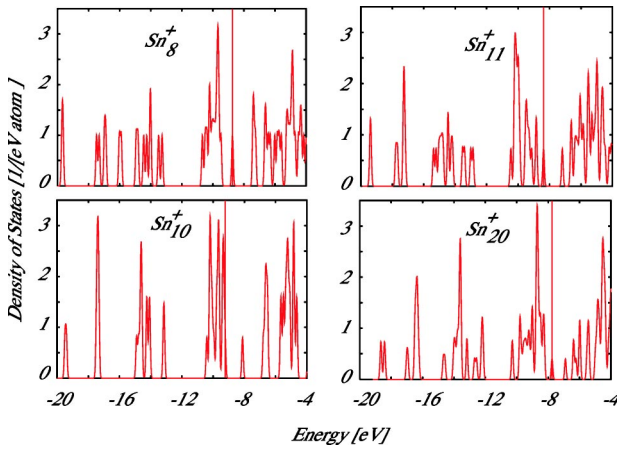

FIG. 5. Plots of the density of states for Sn_8, Sn_{10}, Sn_{11}, and Sn_{20} cation clusters in the lowest energy structures.

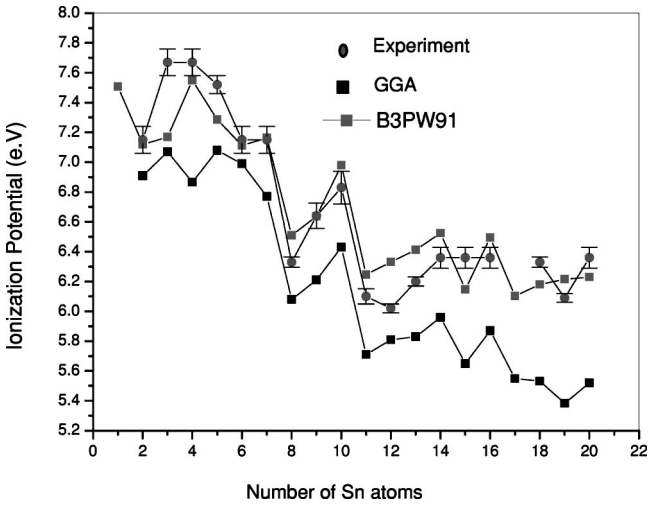

FIG. 6. Comparison of the experimental and calculated IPs of tin clusters.

B3PW91 results represent well the bonding in these clusters. This is important for a proper understanding of the fragmentation behavior of cation clusters. Figure 6 shows the plot of IPs of tin clusters as a function of the cluster size obtained with GGA and B3PW91 functionals. It is seen that the results from the B3PW91 functional are in better agreement with the experimental values. Calculations were also performed on nearly degenerate isomers of 10- and 15-atom clusters in order to check if the cation of another isomer has lower energy. However, we find that the energy ordering of the isomers does not change.

D. Fragmentation of neutral and charged clusters

Table V gives a comparison of the results for a few lowest energy fragmentation channels of cation tin clusters. We have listed the results obtained from B3PW91 and GGA calculations in order to compare with those obtained from surface induced dissociation (SID) experiments on cation clusters.[52] The fragmentation energy is calculated as the lowest energy required to dissociate the parent cation cluster into a neutral part and a cation subcluster. It is found that in both pseudopotential (GGA) and B3PW91 approaches, small clusters with $n \leqslant 11$ favor atom evaporation, while for larger clusters, a fission type fragmentation is more favorable. For Si clusters also fission type fragmentation has been found and it starts from $n=9$ onwards.[54] The experimental results on tin clusters show that the charge should be on the heavier fragment. In GGA, for small clusters, charge is predicted to be on the Sn atom whereas in B3PW91, it is with the heavier fragment, in agreement with experiments. This is due to the better agreement of the IP of Sn atom using the B3PW91 functional with experiment. Sn_{11}^{+} is found to be the largest fragmentation product. As Sn_8^{+} and Sn_{11}^{+} are fragments of larger clusters, this could also lead to their higher abundances under high laser fluence for which fragmentation is more likely to happen. The good agreement with the experimental observations gives us confidence that our search for the lowest energy structures should represent the global minima.

TABLE V. The fragmentation products of cation tin clusters. The first number in the brackets represents the charged fragment while the second number represents the neutral product. The experimental results are from Ref. 52.

n	GGA	B3PW91	Experiment
3	(1,2)	(2,1)	⋯
4	(1,3)	(3,1)	⋯
5	(1,4)	(4,1)	⋯
6	(1,5)	(5,1)	⋯
7	(1,6)	(6,1)	(6,1)
8	(1,7)	(7,1)	(7,1)
9	(8,1),(7.2)	(8,1),(7,2)	(7,2),(8,1)
10	(9,1),(6,4),(8,2)	(9,1),(8,2),(6,4)	(9,1),(8,2),(6,4)
11	(10,1),(7,4),(9,2)	(10,1),(7,4),(9,2)	(10,1),(9,2),(7,4)
12	(7,5),(11,1)(6,6)	(11,1),(7,5),(6,6)	(6,6),(7,5)
13	(7,6)	(7,6)	(7,6)
14	(7,7)	(7,7)	(7,7)
15	(8,7),(9,6)	(8,7)	(8,7)
16	(9,7),(10,6)	(9,7)	(9,7), (10,6)
17	(10,7)	(10,7)	(10,7)
18	(11,7),(8,10),(9,9)	(8,10)	(11,7),(8,10)
19	(9,10),(10,9),(12,7)	(10,9)	(10,9),(6,13) (7,12)
20	(10,10)	(10,10)	(10,10), (7.13)

IV. DISCUSSION AND CONCLUSIONS

We have presented results of the atomic structures of the neutral and cation tin clusters using *ab initio* calculations under the framework of GGA, BLYP, B3LYP, and B3PW91 exchange-correlation functionals. Our results show that the B3PW91 functional provides a good description of bonding in small tin clusters and the calculated fragmentation behavior is in excellent agreement with experiments.[52] For $n \leqslant 11$, both experiment and calculations suggest dissociation of a Sn atom from a cation cluster with charge residing on the heavier fragment to be the most favorable whereas for larger clusters, fragmentation into two subclusters is preferred. A similar fission type fragmentation behavior was obtained for silicon and germanium clusters. It is to be noted that around $n=18-20$ the structures of clusters of all these elements are similar. The IPs obtained from the B3PW91 functional are also in very good agreement with the available experimental data. These represent significant improvement over the values obtained by using GGA. The B3PW91 BEs for very small clusters with $n \leqslant 7$ agree well with the experimental data. However, for larger clusters these are underestimated in B3PW91 whereas GGA results are an overestimate. From this we conclude that correlation effects are stronger in the small size range and that the metallic nature of bonding increases as the cluster size grows. Therefore, for larger clusters, GGA would provide a better representation of the bonding in these clusters as it is also evident from the good agreement with the bulk cohesive energy. Importance of correlation effects has also been noted in small silicon clusters. An important result is that tin clusters tend to have BEs that

are rather closer to the bulk cohesive energy even for small clusters in a size range of about 10–20 atoms than it is normally the case for other metal clusters. But this should be expected due to the lower surface energy of tin. Comparing the BEs of small tin and Al clusters with the corresponding bulk values, we notice that the difference in the case of tin is significantly lower. These results suggest that there is a significant gain in the bond energies due to the change in the structure of the Sn clusters as compared to the bulk fragments as it was reported earlier.[34] This could be responsible for an increase in the melting temperatures of small clusters. The changes in the structures of clusters due to a positive charge are found to be small. The relative stabilities of cation clusters are, however, affected more significantly and this affects the abundances and fragmentation behavior of clusters. We have also calculated the vibrational spectra and the infrared intensities as well as the Raman activities of selected clusters and these can be used to identify from experiments the structures of tin clusters.

ACKNOWLEDGMENTS

C.M. and V.K. acknowledge the kind hospitality at the Institute for Materials Research, Tohoku University and the support of the staff of the Centre for Computational Materials Science at IMR-Tohoku University in making the Hitachi SR2201 and SR8000 parallel machines available and for their cooperation. V.K. also acknowledges support from Japan Society for Promotion of Science (JSPS).

*Email address: chimaju@magnum.barc.ernet.in

[1] V. Kumar, K. Esfarjani, and Y. Kawazoe, in *Clusters and Nanomaterials*, Springer Series in Cluster Physics, edited by Y. Kawazoe and K. Ohno (Springer, Heidelberg, 2002), p. 9.

[2] A. Kasuya, R. Sivamohan, Y. A. Barnakov, I. M. Dmitruk, T. Nirasawa, V. R. Romanyuk, V. Kumar, S. V. Mamykin, K. Tohji, B. Jeyadevan, K. Shinoda, T. Kudo, O. Terasaki, Z. Liu, R. V. Belosludov, V. Sundararajan, and Y. Kawazoe, Nat. Mater. **3**, 99 (2004).

[3] G. Seifert, Nat. Mater. **3**, 77 (2004).

[4] V. Kumar and Y. Kawazoe, Phys. Rev. Lett. **87**, 045503 (2001).

[5] G. von Helden, M. T. Hsu, N. Gotts, and M. T. Bowers, J. Phys. Chem. **97**, 8182 (1993).

[6] M. F. Jarrold and V. A. Cinstant, Phys. Rev. Lett. **67**, 2994 (1991).

[7] M. F. Jarrold and J. E. Bower, J. Chem. Phys. **96**, 9180 (1992).

[8] J. M. Hunter, J. L. Fye, M. F. Jarrold, and J. E. Bower, Phys. Rev. Lett. **73**, 2063 (1994).

[9] A. A. Shvartsburg and M. F. Jarrold, Phys. Rev. Lett. **85**, 2530 (2000).

[10] K. LaiHing, R. G. Wheeler, W. L. Wilson, and M. A. Duncan, J. Chem. Phys. **87**, 3401 (1987).

[11] K. A. Gingerich, A. Desideri, and D. L. Cocke, J. Chem. Phys. **62**, 731 (1975).

[12] T. P. Martin and H. Schaber, J. Chem. Phys. **83**, 855 (1985).

[13] M. Watanabe, Y. Saito, S. Nishigaki, and T. Noda, Jpn. J. Appl. Phys., Part 1 **27**, 427 (1988).

[14] Y. Saito and T. Noda, Z. Phys. D: At., Mol. Clusters **12**, 225 (1989).

[15] G. Gantefor, M. Gausa, K. H. Meiwes-Broer, and H. O. Lutz, Z. Phys. D: At., Mol. Clusters **12**, 405 (1989).

[16] Ch. Luder and K. H. Meiwes-Broer, Chem. Phys. Lett. **294**, 391 (1998)

[17] S. Yoshida and K. Fuke, J. Chem. Phys. **111**, 3880 (1999).

[18] X. Ren and K. M. Ervin, Chem. Phys. Lett. **198**, 229 (1992).

[19] P. Jackson, I. G. Dance, K. J. Fisher, G. D. Willett, and G. E. Gadd, Int. J. Mass Spectrom. Ion Processes **157/158**, 329 (1996).

[20] A. A. Shvartsburg and M. F. Jarrold, Phys. Rev. A **60**, 1235 (1999).

[21] A. A. Shvartsburg and M. F. Jarrold, Chem. Phys. Lett. **317**, 615 (2000).

[22] A. B. Anderson, Chem. Phys. **63**, 4430 (1975).

[23] D. Dai and K. Balasubramanian, J. Chem. Phys. **96**, 8345 (1991).

[24] D. Dai and K. Balasubramanian, J. Phys. Chem. **96**, 9236 (1992).

[25] D. Dai and K. Balasubramanian, J. Phys. Chem. **100**, 19321 (1996).

[26] D. Dai and K. Balasubramanian, J. Chem. Phys. **108**, 4379 (1998).

[27] B. Wang, L. M. Molina, M. J. Lopez, A. Rubio, J. A. Alonso, and M. J. Scott, Ann. Phys. (Leipzig) **7**, 107 (1998).

[28] E. Honea, A. Ogura, C. A. Murray, K. Raghabachari, W. O. Spenger, M. F. Jarrold, and W. L. Brown, Nature (London) **366**, 42 (1993).

[29] S. Li, R. J. Van Zee, W. Weltner, Jr., and K. Raghabachari, Chem. Phys. Lett. **243**, 275 (1995).

[30] C. Xu, T. R. Taylor, G. R. Burton, and D. M. Neumark, J. Chem. Phys. **108**, 1395 (1998).

[31] G. R. Burton, C. Xu, C. C. Arnold, and D. M. Neumark, J. Chem. Phys. **104**, 2757 (1996).

[32] S. Ögüt and J. R. Chelikowsky, Phys. Rev. B **55**, R4914 (1997).

[33] Z.-Y. Lu, C.-Z. Wang, and K.-M. Ho, Phys. Rev. B **61**, 2329 (2000).

[34] C. Majumder, V. Kumar, H. Mizuseki, and Y. Kawazoe, Phys. Rev. B **64**, 233405 (2001).

[35] L. Mitas, J. C. Grossman, I. Stich, and J. Tobik, Phys. Rev. Lett. **84**, 1479 (2000).

[36] G. Kresse and J. Hafner, Phys. Rev. B **47**, 558 (1993); G. Kresse and J. Furthmüller, *ibid.* **54**, 11 169 (1996); Comput. Mater. Sci. **6**, 15 (1996); G. Kresse and J. Hafner, J. Phys.: Condens. Matter **6**, 8245 (1994); Phys. Rev. B **49**, 14 251 (1994).

[37] D. Vanderbilt, Phys. Rev. B **41**, 7892 (1990).

[38] J. P. Perdew, in *Electronic Structure of Solids 1991*, edited by P. Ziesche and H. Eschrig (Akademie Verlag, Berlin, 1991), p. 11.

[39] M. Fuchs, M. Bockstedte, E. Pehlke, and M. Scheffler, Phys. Rev. B **57**, 2134 (1990).

[40] The binding energies and bulk cohesive energy calculated under GGA exchange-correlation functionals are slightly higher than our previously reported values.[34] This discrepancy is due to the difference in the atomic spin-polarization energy, which in-

cluded entropy due to the broadening of the electronic states in our previous calculation.

[41] C. Kittel, *Introduction to Solid State Physics*, 7th ed. (Wiley, New York, 1996), p. 57.

[42] A. Aguado, Phys. Rev. B **67**, 212104 (2003).

[43] B. Liu, Z.-Y. Lu, B. Pan, C.-Z. Wang, K.-M. Ho, A. A. Shvartsburg, and M. F. Jarrold, J. Chem. Phys. **109**, 9401 (1998).

[44] K.-M. Ho, A. A. Shvartsburg, B. Pan, Z.-Y. Lu, C.-Z. Wang, J. G. Wacker, J. L. Fye, and M. F. Jarrold, Nature (London) **392**, 582 (1998).

[45] Gaussian 98 (Revision A.10), M. J. Frisch, G. W. Trucks, H. B. Schlegel, G. E. Scuseria, M. A. Robb, J. R. Cheeseman, V. G. Zakrzewski, J. A. Montgomery, Jr., R. E. Stratmann, J. C. Burant, S. Dapprich, J. M. Millam, A. D. Daniels, K. N. Kudin, M. C. Strain, O. Farkas, J. Tomasi, V. Barone, M. Cossi, R. Cammi, B. Mennucci, C. Pomelli, C. Adamo, S. Clifford, J. Ochterski, G. A. Petersson, P. Y. Ayala, Q. Cui, K. Morokuma, P. Salvador, J. J. Dannenberg, D. K. Malick, A. D. Rabuck, K. Raghavachari, J. B. Foresman, J. Cioslowski, J. V. Ortiz, A. G. Baboul, B. B. Stefanov, G. Liu, A. Liashenko, P. Piskorz, I. Komaromi, R. Gomperts, R. L. Martin, D. J. Fox, T. Keith, M. A. Al-Laham, C. Y. Peng, A. Nanayakkara, M. Challacombe, P. M. W. Gill, B. Johnson, W. Chen, M. W. Wong, J. L. Andres, C. Gonzalez, M. Head-Gordon, E. S. Replogle, and J. A. Pople (Gaussian, Inc., Pittsburgh, PA, 2001).

[46] A. D. Becke, Phys. Rev. A **38**, 3098 (1988); C. Lee, W. Yang, and R. G. Parr, Phys. Rev. B **37**, 785 (1988); A. D. Becke, J. Chem. Phys. **98**, 5648 (1993); K. Burke, J. P. Perdew, and Y. Wang, in *Electronic Density Functional Theory: Recent Progress and New Directions*, edited by J. F. Dobson, G. Vignale, and M. P. Das (Plenum, New York, 1998); J. P. Perdew, J. A. Chevary, S. H. Vosko, K. A. Jackson, M. R. Pederson, D. J. Singh, and C. Fiolhais, Phys. Rev. B **46**, 6671 (1992); **48**, 4978 (1993); J. P. Perdew, K. Burke, and Y. Wang, *ibid.* **54**, 16 533 (1996).

[47] W. R. Wadt and P. J. Hay, J. Chem. Phys. **82**, 284 (1985); P. J. Hay and W. R. Wadt, *ibid.* **82**, 270 (1985); **82**, 299 (1985).

[48] Strictly speaking the ECP will depend upon the type of exchange-correlation functional used. Our usage of the same ECP for different exchange-correlation functionals as implemented in the Gaussian-98 program may have some effects on the final results.

[49] The energies of atoms in the Gaussian program are not given properly as fractional occupations are not treated. This will lead to slight overestimation of the BEs obtained by the Gaussian method. It can also lead to small changes when different basis sets or exchange-correlation functionals are used. However, the relative energies and the trends would not be affected.

[50] The actual curve is likely to be oscillatory. However, we trust that the results shown in the graph are a reasonable representation of the energies of larger clusters.

[51] V. Kumar, S. Bhattacharjee, and Y. Kawazoe, Phys. Rev. B **61**, 8541 (2000).

[52] Y. Tai, J. Murakami, C. Majumder, V. Kumar, H. Mizuseki, and Y. Kawazoe, J. Chem. Phys. **117**, 4317 (2002).

[53] C. Majumder, V. Kumar, H. Mizuseki, and Y. Kawazoe, Chem. Phys. Lett. **356**, 36 (2002).

[54] K. Raghavachari and C. M. Rohlfing, Chem. Phys. Lett. **143**, 428 (1988).